Proceedings of the 7th International Symposium on Cavitation
CAV2009 – Paper No. ##
August 17-22, 2009, Ann Arbor, Michigan, USA

Modeling collapse aggressiveness of cavitation bubbles in hydromachinery

Patrik Zima
Department of Thermodynamics
Institute of Thermomechanics
Academy of Sciences, v. v. i.
Dolejškova 5, 18200 Praha
Czech Republic

Milan Sedlář
SIGMA Research and
Development Institute, s. r. o.
Jana Sigmunda 79, 78350 Lutín
Czech Republic

Miloš Müller
Faculty of Mechanical
Engineering
Technical University of Liberec
Hálkova 6, 46117 Liberec
Czech Republic

ABSTRACT

A simple model of assessment of collapse aggressiveness of cavitation bubbles suitable for application at pump design stage is proposed. The model is focused on quantifying the energetic effects of single bubble collapses and the emphasis is placed on computational efficiency. The objective of the model is to provide a rapid estimation of the erosion risk for steady-state or near-steady-state flow with traveling bubble cavitation. The proprietary 3-dimensional Navier-Stokes code for turbulent flow in hydrodynamic machinery is coupled with the unreduced Rayleigh-Plesset equation for incompressible liquid by virtue of the iterations of continuity and momentum equations to account for density changes in the bubbly regions (two-way coupling). The model of collapse aggressiveness of the cavitation bubbles is based on the estimation of the energy dissipated between two successive bubble rebounds. The model is tested for a 2-dimensional hydrofoil in the cavitation tunnel of SIGMA Research and Development Institute in Lutín. The closed-loop tunnel is equipped with the acoustic bubble spectrometer to measure the nuclei population in the test section inlet. The erosion pattern of the hydrofoil surface is monitored using optical profilometry. The results indicate the dominant effect of the first (most energetic) collapses, however, the model overestimates the importance of smaller nuclei mainly due to their large number in the spectra. Introduction of a threshold for the minimum collapse energy required to form any erosive potential seems necessary to rectify this deficiency. The model, although aimed to achieve efficiency and simplicity by relying on the single-bubble dynamics, shows good agreement with the experimental evidence. An attempt to apply the model to the 3-dimensional geometry of a mixed-flow pump impeller is also presented.

This paper is a report on part one of work in progress. In the second part the results of the ongoing pitting tests will be used to develop a model of erosive potential.

INTRODUCTION

The erosion of the blade material in hydraulic devices is caused by violent collapses of vapor structures [1] in the vicinity of the blade surface. In most situations, these vapor structures are identified as transient cavitation bubbles, however, other erosive mechanisms can be observed such as collapses of large vapor-filled cavities or bubble clouds enhancing the single-bubble collapses as a result of shock waves originated from the center of the collapsing cloud [2]. The modeling of the process is complicated as it requires the knowledge of the response of the solid material. The initial bubble population (nuclei content) in the inlet flow to the hydrodynamic device is often either unknown (especially at design stage) or expensive to obtain experimentally. The phenomenon typically occurs in a complex 3-dimensional geometry and a turbulent flow. Bubbles tend to depart from their spherical shape due to shear stress in the flowing liquid. The erosion itself is caused by microscopic liquid jets [3] removing pieces of material fatigued by repetitive action of the shock waves generated instantly after the violent collapses. The velocity of the liquid microjet was estimated in [4] and the analysis served as the basis for the estimation of the impact pressures by use of the water-hammer formula. The numerous attempts to predict the magnitude of cavitation erosion or cavitating flow aggressiveness include the approach found in [5], which is based on the relation between the volume of transient cavities and its rate of production to the material deformation energy, and the approach found in [6], which is based on evaluating the profile and the energy of the pressure waves emitted during cavity collapse. Most recently, an erosion model coupled with the 2-dimensional CFD tool based on the barotropic state law was examined in [7] for unsteady cavitation with periodic vapor shedding. Enhancement of the single-bubble collapses by the shock wave from the collapsing bubble cloud was identified as the main erosion mechanism. As shown in [8], the impact loads generated by the collapsing bubbles must be measured for the material in question and different cavitation intensities in order to obtain any reliable prediction on the erosion parameters (such as incubation period or erosion rates). In [9] it has been shown that the flow aggressiveness can be determined from the pitting tests using the material properties to obtain these impact loads. Typically,

the performance of impact load measurement, pitting tests and nuclei population measurement is associated with significant experimental expenses. According to our experience, without having all these expensive experimental data available for every tested case any quantitative data obtained from the various models of cavitation flow aggressiveness have a mainly comparative value.

For the reasons outlined above, we look for a computationally inexpensive approach suitable for the design stage, where no measurements of impact loads, erosion rates or nuclei population are available. In the present work, we will limit ourselves to cavitating flows where the erosion of the solid surface can be attributed to collapses of individual traveling bubbles. In hydrodynamic devices, such as water pumps, this regime is characteristic for low angles of attack and cavitation intensities. For this purpose the use of the Rayleigh-Plesset equation is justified due to its relative simplicity.

NUMERICAL SOLVER FOR MAIN FLOW

The main flow is analyzed using the SIGMA proprietary numerical code suitable for pump flows. The code is described in [10] and [11] and it has been validated on numerous experiments. Here, only a basic description of the method will be given. The flow is modeled using the 3-dimensional Reynolds-averaged Navier-Stokes equations for one blade-to-blade passage. The computational domain is discretized using the Finite Element Method with penalization and reduced integration applied to linear hexahedron elements. The changes of density in the bubbly regions are taken into account using the generalized form of the penalty formulation. The turbulence is modeled using the high-Reynolds-number k-ε model. In this work, the code is applied to a 2-dimensional problem (a flow past hydrofoil) as well as a 3-dimensional problem (flow in a pump impeller).

COUPLING OF THE BUBBLE DYNAMICS WITH THE MAIN FLOW SOLVER

Owing to our interest in a simple and efficient method for assessing the collapse aggressiveness, we confine ourselves to the employment of the Rayleigh-Plesset equation for spherical bubbles. Naturally, this limits the applicability of the model to steady-state or near-steady-state traveling bubble cavitation and for situations where other effects enhancing the bubble collapse such as collapses of remnant bubble clouds or periodic vortex shedding are not observed. According to our experience, these adverse phenomena can be avoided when hydraulic devices are operated near the design point. Accordingly, bubble fission or coalescence and bubble-bubble interactions are neglected. The bubbles across the inlet to the computational domain are distributed uniformly. The nuclei population in the inlet flow is either measured by acoustic spectrometry in the cavitation tunnel described later in this paper or taken from the literature. The following Rayleigh-Plesset equation for compressible liquid is used to describe the dynamics of cavitation bubbles of different initial radii [12]:

$$R\ddot{R}+\frac{3}{2}\dot{R}^2+\frac{4\nu_l\dot{R}}{R}+\frac{2S}{\rho_l R}\left(1-\left(\frac{R_0}{R}\right)^{3\gamma-1}\right)=$$

$$=\frac{p_v-p_{l0}}{\rho_l}\left(1-\left(\frac{R_0}{R}\right)^{3\gamma}\right)+\frac{p_0-p_{l\infty}}{\rho_l}+\frac{R}{\rho_l c_l}\frac{D}{Dt}\left(p_g-p_{l\infty}\right) \quad (1)$$

The initial partial pressure of the non-condensable gas p_{g0} is determined from the equilibrium conditions [1] as

$$p_{g0}=p_{l0}+\frac{2\sigma}{R_0}-p_v \quad (2)$$

The above assumption is justified because the water in the cavitation tunnel is not deaerated during the experiment and the initial microbubbles (in the inlet flow) can be assumed to be in equilibrium at the initial liquid pressure p_{l0}.

The coupling of Eq. 1 with the Navier-Stokes equations is achieved using the Euler-Lagrange approach (two-way coupling) described in [13]. First, the streamlines are obtained using the Navier-Stokes code. The different values of the bubble initial radius from the measured bubble spectrum are assigned to each streamline of the computational domain equitably to satisfy the assumption of uniform nuclei population in the inlet cross-section. The Eq. 1 is then integrated along all streamlines for each bubble of the initial nuclei spectrum using the adaptive step size algorithm. The volume fraction is calculated to obtain the main flow density distribution, which is then used to reiterate the continuity and momentum equations for the main flow. Once the reiteration process is completed, the streamlines to be examined for bubble collapses are identified. For the study of collapse aggressiveness only carefully selected streamlines near the solid boundary are considered. Finally, the points of all bubble collapses on these streamlines are identified and the collapse aggressiveness is evaluated using the model described in the next section.

MODEL OF COLLAPSE AGGRESSIVENESS

The energy dissipated during the *i*-th collapse of a single bubble is obtained by subtracting the values of the work W_{growth} for two successive maxima of the bubble radius. W_{growth} is obtained as the work done by the pressure inside the bubble p_B against the ambient liquid pressure $p_{l\infty}$ to expand the bubble from the minimum (or initial) radius $R_{\min}$ to the maximum radius $R_{\max}$ [14] if the liquid surface tension, viscosity and compressibility are neglected:

$$W_{growth}=\int_{R_{\min}}^{R_{\max}}4\pi R^2\left(p_{l\infty}-p_B\right)dR \quad (3)$$

The two pressures p_B and $p_{l\infty}$ and the radius of the bubble R are determined from the numerical solution of the turbulent pump flow and Eq. 1. The energy dissipated during the collapse is obtained by subtracting the values of the work described in Eq. 3 for the two successive maxima of the radius. For example, for the first collapse, we subtract the work for the expansion from the initial radius R_0 ($= R_{min1}$) to the first maximum R_{max1} and the work for the expansion from the first collapse radius R_{min2} to the second maximum R_{max2}. The energy dissipated during the i-th collapse is then given by:

$$E_{ii+1} = W_{growth}\Big|_{R_{\min i}}^{R_{\max i}} - W_{growth}\Big|_{R_{\min i+1}}^{R_{\max i+1}} \quad (4)$$

An unknown part of this energy denoted as E_{EP} has an erosive potential expressed using the factor K:

$$E_{EP} = K E_{ii+1} \quad (5)$$

The energy defined by Eq. 4 breaks up into several components. As shown in [14], the largest portion of the energy is dissipated in the form of a shock wave propagated from the bubble center at the beginning of the rebound phase. Since only one half of the shock wave energy is directed towards the blade surface (the other half is emitted into the liquid) we can safely assume that $K \leq 1/2$. In principle, the factor K depends on a number of parameters including the bubble contents, liquid properties, evaporation/condensation rate etc., of which some of them are difficult to obtain from the numerical simulation, such as the bubble standoff distance (ratio of the distance of the bubble center from the blade surface during the collapse and the maximum bubble radius). Therefore, due to lack of further knowledge and for the purpose of our model evaluation we choose $K = 1/2$ as the our first arbitrary approximation.

The values of E_{EP} are calculated for each bubble collapse, summed up for all bubbles along each streamline and expressed as the power per unit area (or E_{EP} per unit area and time, based on the local flow velocity) denoted $\dot{e}_{EP}$. It should be emphasized here again that the term "erosive potential" is in fact a measure of bubble collapse aggressiveness. Its relation to common erosion parameters (such as incubation period or erosion rate) is not straightforward. According to [15] the most important factor of the energy lost during the collapse is associated with the liquid microjet impact. The other factors are acoustic radiation, shock waves, viscous dissipation and heat transfer. We have shown in [14] for a bubble collapsing far from the solid surface that the energy of the emitted shockwave is roughly equal to the energy described in this model.

EXPERIMENTAL SETUP

The experiments were conducted in the SIGMA Research & Development Institute on a horizontal closed-loop water cavitation tunnel for isolated 2-dimensional and 3-dimensional hydrofoils. The schematic of the tunnel is shown in Fig. 1. The parameters of the tunnel are summarized in Tab. 1.

The test section is shown in Fig. 2 with inner dimensions 150 × 150 × 500 mm. All sides of the test section are transparent to allow observation and recording of the flow pattern using a video camera. The flow rate is controlled by the variable-speed driven axial-flow pump. The maximum flow rate is 0.55 m^3/s and the maximum velocity at the inlet of the test section is 24.5 m/s. The capacity of the main tank equipped with two sets of honeycombs is 35 m^3. The compressor and vacuum pumps in the closed loop generate different pressure levels while maintaining constant volume flow rate. The transit time of a fluid particle through the loop is 72 s for the maximum flow rate. The maximum span of the hydrofoil is 150 mm. The hydrofoil mounts allow to vary the angles of attack between 0˚ and ±180˚. The nuclei content in the bypass line upstream of the test section was measured using the Dynaflow acoustic bubble spectrometer (ABS). Two sets of hydrophones were used (50 and 150 kHz). The pit development on the hydrofoil surface was monitored using the FRT optical profilometer at regular time intervals.

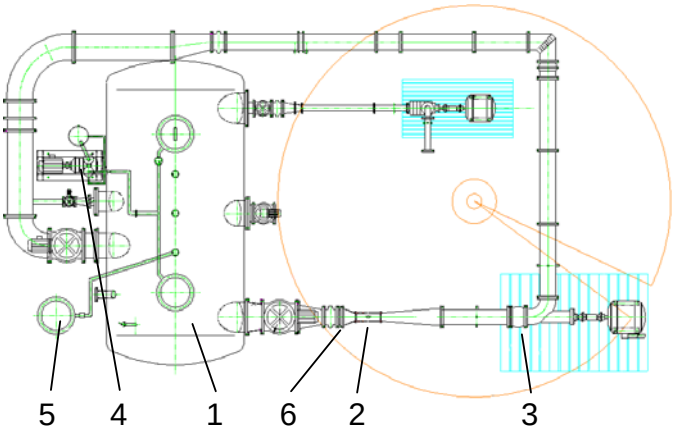

Figure 1: Water cavitation tunnel in SIGMA R&D Institute in Lutín. 1 – reservoir, 2 – test section, 3 – axial-flow pump, 4 – vacuum pump, 5 – compressor, 6 – bypass connection to acoustic bubble spectrometer.

Table 1. Main parameters of the water cavitation tunnel in SIGMA Research & Development Institute in Lutin.

Tunnel type:	Closed-loop
Reservoir volume:	35 m^3
Particle transit time:	72 s (max. flow rate)
Test section (h x w x l)	150 x 150 x 500 mm
Maximum velocity at the inlet to the test section:	24.5 m/s
Maximum flow rate:	0.55 m^3/s
Range of incidence angles:	0±180°

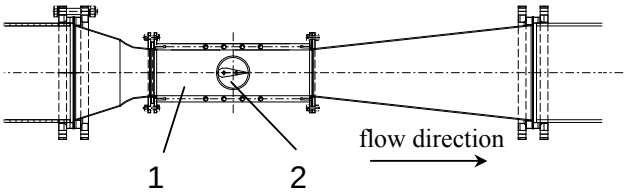

Figure 2: Test section of the cavitation tunnel. 1 – Plexiglas walls, 2 – hydrofoil.

2-DIMENSIONAL CASE: EXPERIMENTAL RESULTS

The experiments were conducted for the 2:3 semi-elliptic nose/NACA 0020 tail prismatic hydrofoil shown in Fig. 3. The chord length of the hydrofoil is 100 mm and the span is 150 mm. First, an aluminium hydrofoil was used to confirm the regime of traveling bubble cavitation for low angles of attack and to test the optical profilometry configuration for a material that requires relatively short times to obtain measurable pits.

Then, a cast-iron hydrofoil was mounted in the test section with the angle of attack –1°. The flow rate was set to 0.22 m^3/s and the pressure measured upstream of the hydrofoil was 94 kPa. The corresponding velocity of the undisturbed flow was 9.8 m/s. The cavitation number is based on the pressure at the inlet of the test section $p_{l\infty}$ and on the vapor pressure p_v divided by the dynamics pressure (defined by the liquid density ρ_l and the upstream flow velocity v):

$$\sigma = \frac{(p_{l\infty} - p_v)}{\frac{1}{2}\rho v^2} \tag{5}$$

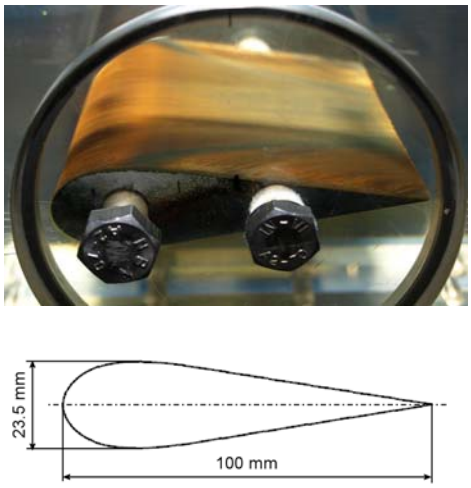

Figure 3: Geometry of the tested hydrofoil and its mount position in the test section of the cavitation tunnel.

The cavitation number was $\sigma = 1.93$ for all tests. The bubble spectra obtained by the acoustic bubble spectrometer are shown in Fig. 4. Two tests were conducted (denoted as Sigma1 and Sigma2), each with 10 series of 30 sample measurements (i.e. 300 samples per test). For reference, the measured bubble spectra are compared with the spectra obtained by [16] for air bubbles injected in the flow through micro-porous tube and [17] for air bubbles entrained downstream of a hydraulic jump. The systematic jump in the number of bubbles in the range 60-75 μm and a missing spectrum of bubble radii below 25 μm is probably caused by the fact that the two hydrophones used for the measurement do not fully cover the examined range of bubble radii. In order to overcome the current deficiency in the spectrometer setup and for the purpose of our immediate numerical analysis, the data measured in the SIGMA cavitation tunnel were interpolated between 50 and 80 μm and extrapolated to 15 μm (the smallest bubble radius sampled by the current spectrometer setup, however, with no detected signal) using the piecewise interpolation of the type 10^{x^2} ("quadratic" in the logarithmic scale).

Fig. 5 shows the short-exposure photograph of the traveling bubble cavitation on the leading edge of the hydrofoil under conditions described in this section. The maximum radius of the largest bubble in the numerical calculation was 2.5 mm, whereas the maximum observed radius of a bubble determined from the photograph is 2.5–3.0 mm, which shows a very good agreement. The small difference can be attributed to the slight deformation of the largest observed bubbles.

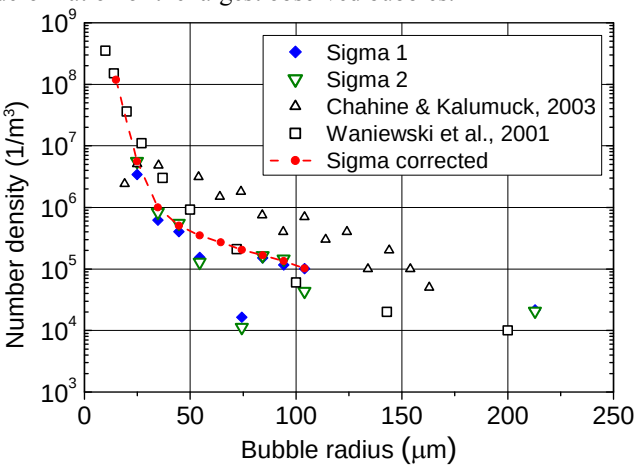

Figure 4: Bubble spectra in the inlet flow upstream of the test section measured by the acoustic bubble spectrometer and compared with the measurement found in [16] and [17].

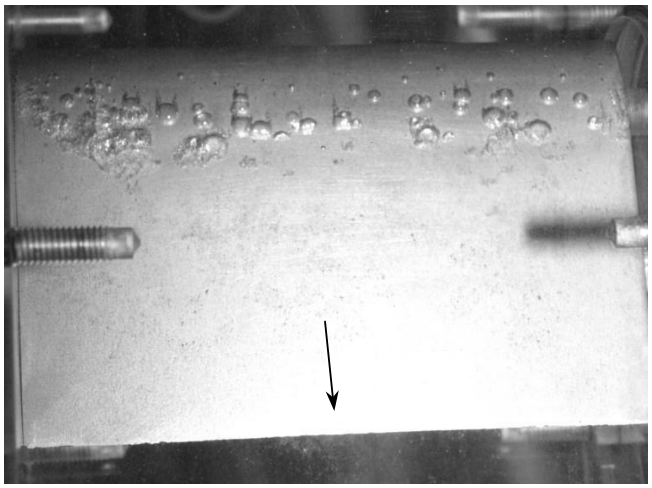

Figure 5: Cavitating flow on the upper (pressure) side of the hydrofoil. The direction of the flow is from top to bottom.

The pitting test was repeated twice for the same setup. The hydrofoil was removed for inspection by the FRT optical profilometer at predefined intervals. The number density, characteristic pit sizes and depths were measured typically on a surface area 8 x 4 mm with the scanning resolution 5 μm. Fig. 6a shows the photograph of the eroded surface of the cast-iron hydrofoil in the second stage of erosion (steady state volume loss rate). The cavitation damage is located on a narrow strip of surface between 27% and 31.5% of the chord length of the upper surface and between 31% and 36.5% on the lower surface. Fig. 6b shows the bitmap of the pits from Fig. 6a represented by dark pixels and the relative surface area of the pits defined as the local percentage of the surface area covered by pits. The highest relative surface area is 35% and is located

almost in the middle of the eroded pattern, although the pits are not distributed symmetrically in the streamwise direction as a small number of pits can be found downstream of the eroded area.

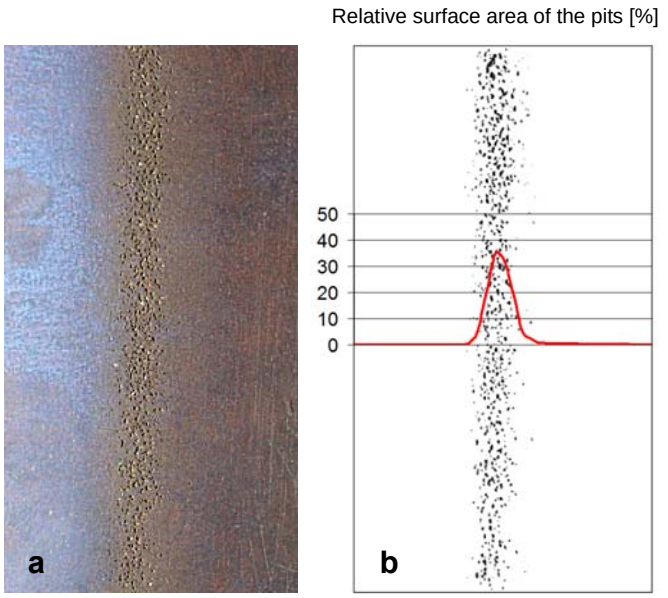

Figure 6: a) Cavitation damage on the upper (pressure) side of the cast-iron hydrofoil in the second stage of erosion (steady state volume loss rate); b) Map of the pits and the corresponding percentage of the surface area covered by pits.

2-DIMENSIONAL CASE: CFD ANALYSIS

The cavitating flow around the hydrofoil described in the previous section was examined using the proposed numerical approach. The computational domain was discretized using 200,000 hexahedron elements. For the assessment of the collapse aggressiveness, only the mid-span streamlines were considered in order to filter out the influence of 3-dimensionality of the flow close to the side walls. The nuclei population denoted as "Sigma corrected" in Fig. 4 was used.

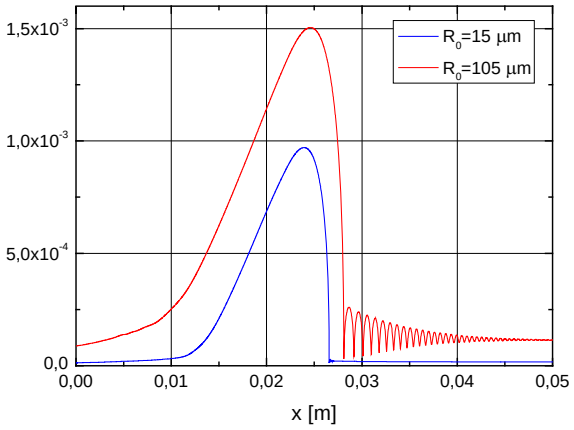

Figure 7: Typical evolutions of bubble radius along the mid-span streamline on the upper side of the hydrofoil for selected initial bubbles radii.

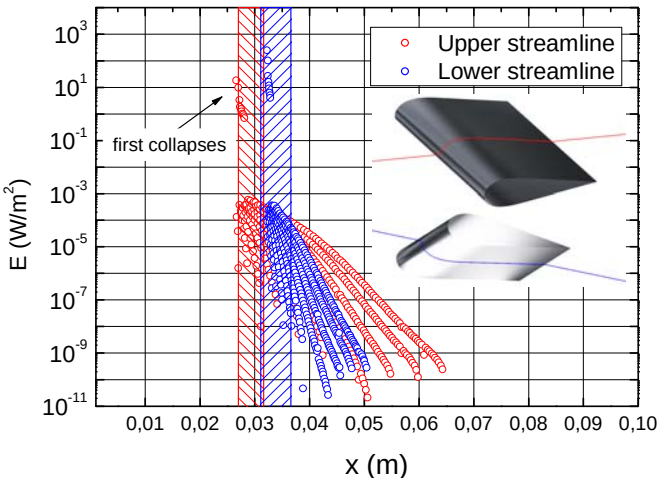

Figure 8: The power per unit area dissipated during the bubble collapses along the mid-span computational streamlines on the upper (red) and lower (blue) side of the hydrofoil. The hatched areas of the corresponding color denote the position of the eroded area in the stage of steady-state erosion rate.

In our experiment macroscopic bubbles appeared only in the vicinity of the hydrofoil surface. Therefore, for the assessment of collapse aggressiveness of the cavitation bubbles only the streamlines near the surface were considered. The standoff distance of these "surface" streamlines in the location of first collapses is roughly equal to the maximum radius of the largest bubble in the region of its maximum expansion. In addition, a zero pressure gradient across the boundary layer is assumed. Fig. 7 shows the typical evolutions of the bubble radius along the mid-span streamline on the upper side of the hydrofoil for selected initial bubble radii. Fig. 8 shows the quantity from Eqs. 3-5 per unit time and area along the streamlines on the upper (red) and lower (blue) side of the hydrofoil. The first (most violent) collapses of the cavitation bubbles are found at the distance 26-28% of the chord length for the upper side and at 32-33% on the lower side. The subsequent collapses are located downstream of these distances and are many orders of magnitude less energetic than the first collapses. According to the results, the highest erosion potential of the first collapses is carried by the smallest bubbles owing to their large number in the spectrum. By comparison of Figs. 6b and 8 we see that the experimental results exhibit a maximum whereas the numerical results predict decreasing erosive potential in the downstream direction. This can be explained as follows: Because the real flow is not perfectly steady the positions of the collapses fluctuate around the point (in fact the line) of highest damage. The measured distribution of pits in Fig. 6b is a consequence of this fluctuation.

3-DIMENSIONAL CASE: CFD ANALYSIS

In this section, the numerical approach described above is demonstrated on the case of cast-iron mixed-flow water pump impeller shown in Fig. 9. The pump was designed to operate without boundary layer separation at the design point. The pump was operated at 65-90% of its optimum flow rate (i.e. the flow rate with maximum overall efficiency) for most of its

service life until the rupture of the blades. The estimated cavitation number of the flow was $\sigma = 0.35$. In our CFD analysis, the inlet pressure and flow rate were set to the real operating conditions of the pump and the properties of water were evaluated at 20°C. The computational domain was discretized by H-type structured grid with 80,000 nodes with a simple I-grid in the trailing edge region. Due to lack of reference data, the inlet nuclei content was assumed according to [17] with the corresponding initial volume fraction 0.002%.

Figure 9: a) Cast-iron mixed-flow water pump impeller after service life. The white lines denote the region of the first collapses obtained by CFD. b) Computational geometry of the same impeller with the investigated computational streamlines.

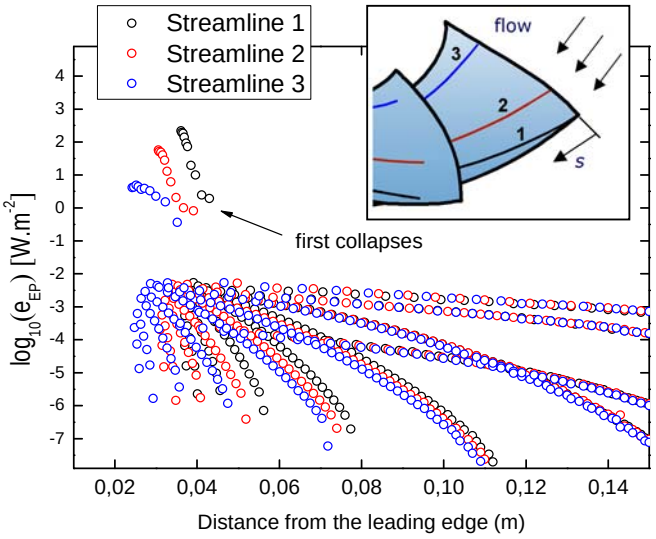

Figure 10: Values of collapse power per unit area $\dot{e}_{EP}$ along three selected streamlines (1, 2 and 3) on the surface of the impeller blade.

Fig. 10 shows the cumulative erosion potential (collapse aggressiveness) per unit area per unit time along 3 selected streamlines on the blade surface shown in the inset figure (about 1/3 of the total blade length). The region of the first (strongest) collapses is denoted by the white lines shown in Fig. 9a. The highest erosion risk is predicted near the outer blade diameter and is associated with the first collapses. The aggressiveness of the subsequent collapses is several orders of magnitude smaller. Similar to the 2-dimensional problem, the highest values of erosion potential are predicted for the smallest bubbles due to their large populations.

CONCLUSION

The presented model of collapse aggressiveness of cavitation bubbles provides a computationally efficient quantitative information about the energy of collapses of cavitation bubbles. The method suggests a dominant importance of the first collapses and the importance of smaller nuclei is overestimated mainly due to their large number in the spectra. For the numerical prediction of the actual erosion pattern it seems sufficient to determine the position and intensity of the first collapses and include consideration of the scatter of the impact positions due to flow rate fluctuations. The quantity proposed for the assessment of the collapse aggressiveness presently does not directly relate to erosion rates and requires scaling based on the ongoing pitting tests. The application of the method to 3-dimensional geometry was demonstrated, however, without reference experimental data. After careful examination of the cavitating conditions the model can be used for determining the flow aggressiveness of traveling bubble cavitation with steady-state or near steady-state flow with low cavitation intensities such as near the design point in hydraulic machinery.

ACKNOWLEDGMENTS

The authors wish to thank the Czech Science Foundation for providing financial support for grant 101/07/1612 and the support of the Research Plan AV0Z20760514 of the Institute of Thermomechanics ASCR, v. v. i. and MSM 4674788501 of the Technical University of Liberec.

NOMENCLATURE

c	[m/s]	=	speed of sound
$\dot{e}$	[W/m^2]	=	power per unit area
E	[J]	=	energy
K	[-]	=	arbitrary factor (constant)
N	[m^{-3}]	=	number of bubbles per unit volume
p	[Pa]	=	pressure
R	[m]	=	bubble radius
S	[N/m]	=	surface tension
s	[m]	=	streamwise coordinate
W	[J]	=	work
x	[m]	=	coordinate in the flow direction
γ	[-]	=	polytropic index of gas
ν	[m^2/s]	=	liquid kinematic viscosity
ρ	[kg/m^3]	=	density
σ	[-]	=	cavitation number

Subscripts

B	=	bubble content
g	=	non-condensable gas
l	=	liquid
0	=	initial (equilibrium) value
v	=	vapor
∞	=	value in infinity

REFERENCES

[1] Franc, J. P. and Michel, J. M., 2004, *Fundamentals of Cavitation*, Kluwer Academic Publishers.

[2] Dular, M., Bachert, B., Stoffel, B., Sirok, B., 2004, Relationship between cavitation structures and cavitation damage, *Wear*, 257, 1176–1184.

[3] Benjamin, T.B., Ellis, A.T., 1966, "The collapse of cavitation bubbles and the pressures thereby produced against solid boundaries," *Philosophical Transactions of the Royal Society of London*, 260, 221–240.

[4] Plesset, M.S., Chapman, R.B., 1971, Collapse of an initially spherical vapor cavity in the neighborhood of a solid boundary, *J. Fluid Mech.*, 47, 283–290.

[5] Pereira, F., Avellan, F., Dupont, Ph., 1998, "Prediction of cavitation erosion: an energy approach," *Journal of Fluids Engineering*, 120, 719–727.

[6] Fortes-Patella, R. *et al*, 2001, "Cavitation Erosion Mechanism: Numerical Simulations Of The Interaction Between Pressure Waves And Solid Boundaries," 4th Intl. Symposium on Cavitation, California Institute of Technology, Pasadena, California, USA, 2001.

[7] Dular, M., Coutier-Delgosha, O., 2009, "Numerical modelling of cavitation erosion," *Intl. J. for Num. Meth. Fluids*, published online in Wiley InterScience.

[8] Hattori, S., Hirose, T., Sugiyama, K., 2009, "Prediction Method for Cavitation Erosion Based on Measurement of Bubble Collapse Impact Loads," The 6th Intl. Symposium on Measurement Techniques for Multiphase Flows, *Journal of Physics: Conference Series*, vol. 147.

[9] Berchiche, N., Franc, J. P., Michel, J. M., 2002, "A Cavitation Erosion Model for Ductile Materials," *J. Fluids Engineering*, 124, 601-606.

[10] Sedlář, M., 1993, "Calculation of Quasi-Three-Dimensional Incompressible Viscous Flows by the Finite Element Method," *Int. J. Numerical Methods in Fluids*, 16, 963.

[11] Sedlář, M., 1997, "Numerical Analysis of Three-Dimensional Turbulent Flow in the Pump Impeller at Partial Load," 10th Conf. on Num. Methods in Laminar and Turbulent Flow, Univ. of Swansea, 10, 97-104.

[12] Hilgenfeldt, S. et al, 1998, "Analysis of Rayleigh-Plesset dynamics for sonoluminescing bubbles," *J. Fluid Mech.*, 365, 171-204.

[13] Zima, P., Sedlář, M., Maršík, F., 2005, "Bubble Creation in Water with Dissolved Gas: Prediction of Regions Endangered by Cavitation Erosion," In: Water, Steam, and Aqueous Solutions for Electric Power. Advances in Science and Technology, Kyoto, Maruzen Co., Ltd., 232-235.

[14] Müller, M., 2007, "Dynamic behaviour of cavitation bubbles generated by laser," Ph.D. dissertation, Faculty of Mech. Engineering, Technical University of Liberec.

[15] Blake, J. R., Pearson, A., Otto, S. R., 2001, "Boundary Integral Methods for Cavitation Bubbles Near Boundaries," 4th Int. Symposium on Cavitation, 2001, California Institute of Technology, Pasadena, USA.

[16] Chahine, G. L., Kalumuck, K. M., 2003, "Development of a near real-time instrument for nuclei measurement: the ABS Acoustic Bubble Spectrometer®," Proc. of Intl. Symposium on Cavitation Inception, 4th ASME/JSME Joint Fluids Engineering Conference, Honolulu, Hawaii, USA, 2003.

[17] Waniewski, T. A., Hunter, Ch., Brennen, Ch. E., 2001, "Bubble measurement downstream of hydraulic pumps," *Int. J. Multiphase Flow*, 27, 1271-1284.